MULTI-FRAME SUPER-RESOLUTION FOR TIME-OF-FLIGHT IMAGING

Fengqiang Li, Pablo Ruiz, Oliver Cossairt, Aggelos K. Katsaggelos

Dept. of Electrical Eng. and Computer Science, Northwestern University, Evanston, IL, 60208

ABSTRACT

Recently, time-of-flight (ToF) sensors have emerged as a promising three-dimensional sensing technology that can be manufactured inexpensively in a compact size. However, current state-of-the-art ToF sensors suffer from low spatial resolution due to physical limitations in the fabrication process. In this paper, we analyze the ToF sensor's output as a complex value coupling the depth and intensity information in a phasor representation. Based on this analysis, we introduce a novel multi-frame superresolution technique that can improve both spatial resolution in intensity and depth images simultaneously. We believe our proposed method can benefit numerous applications where high resolution depth sensing is desirable, such as precision automated navigation and collision avoidance.

***Index Terms*—** Multi-frame Superresolution, Time-of-flight Imaging, Complex Model.

1. INTRODUCTION

In recent years, the problem of acquiring a 3D depth map of a scene has been studied extensively in the field of image processing. A depth map provides a 3D model of the visible surfaces in a scene [1], which makes it very useful in many areas of interest, such as robotics [2], video gaming [3] or biomedical imaging [4]. Some of these applications have led companies like *Oculus* (Virtual Reality), *Snapchat* (Augmented Reality), or *Tesla* (self-driving autonomus cars) to be amongst the most successful companies. Many approaches have been proposed in the literature to acquire a depth map, for instance, light detection and ranging (LIDAR) devices [5], structured light [6], or stereo [7].

One of the most recent techniques is time-of-flight (ToF) sensors [3] which captures both an intensity image and a depth map of the scene at the same time. Three-dimensional (3D) imaging using ToF sensors has rapidly gained widespread adoption in many applications due to their cost effectiveness, simplicity, and compact size. However, the current generation of ToF cameras (e.g., Microsoft Kinect Sensor, 640× 480 pixels [3]) suffers from low spatial resolution compared to regular CCD/CMOS sensors (easily larger than 1000 × 1000 pixels) due to physical limitations in the fabrication process. In this work we propose a novel approach to jointly increase the resolution of a depth map and intensity image provided by a ToF camera.

The process of obtaining a high resolution (HR) image from a set of low resolution (LR) observations is called super-resolution (SR) in image processing [8]. The key question in SR problems is how to reconstruct the sub-pixel information which is missing in the observed LR measurement images. Different approaches are proposed in the literature to perform SR on depth maps acquired by ToF cameras. One strategy to recover sub-pixel information is to use other

This work was supported in part by NSF CAREER grant IIS-1453192, ONR grant N00014-15-1-2735, and DARPA REVEAL grant HR0011-16-C-0028.

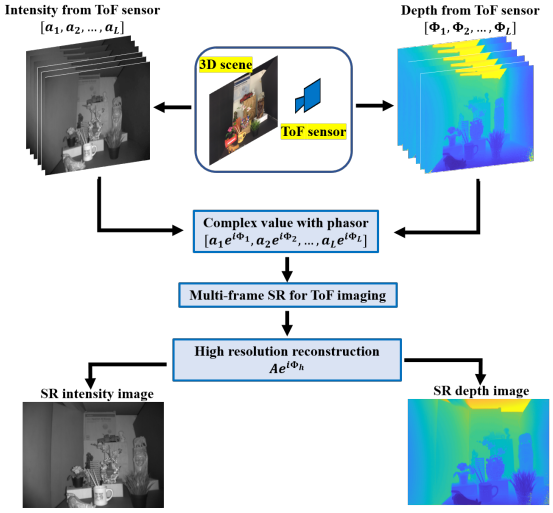

Fig. 1. **Overview of the Multi-frame SR for ToF imaging:** The ToF sensor generates both the intensity and phase images simultaneously when imaging a scene. We combine the intensity output and the phase output to a complex value with phasor. We then extend the multi-frame SR technique to these low-resolution ToF complex outputs. A high resolution reconstruction ($Ae^{i\Phi_h}$) is obtained. We then get the SR intensity and phase images.

imaging modalities. For instance, Ti *et. al.* [9] proposed a photometric stereo technique to improve the ToF spatial resolution. Kadambi *et. al.* [10] combined shape from shading with high spatial resolution to boost the low spatial resolution depth measurement from the ToF sensor. Hui *et al.* [11] use an HR intensity image of the same scene, and Li *et al.* [12] also use compressive sensing to increase the spatial resolution. In both cases the underlying idea is the edges in the depth map can be improved using the information that is provided by either the HR intensity image or optical multiplexing. Although these methods help improve the spatial resolution in depth images, they require extra hardware (e.g., an additional HR RGB camera). Numerous single image SR approaches exist as well, for example Xiao *et al.* [13] apply a bicubic interpolation to obtain a higher resolution depth map, followed by deblurring to obtain a SR reconstruction.

In this paper, we focus on multi-frame (MF) approaches, where sub-pixel information is extracted from a set of LR measurement images of the same scene with small movements between them. This method has been widely used for intensity sensors (see [8, 14, 15]). Recently, this technique has been applied on Google's pixel 3 to improve the lateral resolution [16]. A natural question is whether we can apply multi-frame SR techniques to ToF imaging to improve the spatial resolution of captured depth maps. While previous multiframe ToF techniques (e.g., [11] and [17]) have focused on fusing multiple images taken from different types of cameras, we focus here on the problem of recovering an SR depth map directly from mul-

tiple frames captured by one or more ToF cameras. Our approach takes advantage of the fact that ToF cameras produce both LR intensity images and LR depth maps, avoiding the need for additional HR sensors. Efficient implementation of our multiframe SR technique relies on a linear forward model relating the scene to sensor measurements. While the transform-domain sparsity of natural images applies to depth images, the depth is non-linearly related to the intensity measured at each pixel on a ToF sensor. In this paper, we adopt the phasor representation [18] to model the ToF imaging output as a complex value ($ae^{i\Phi}$) with intensity as amplitude (a) and depth as phase ($e^{i\Phi}$). A linear forward model from the scene to the ToF sensor is generated which is the same as the one used in regular CCD/CMOS sensors. The LR intensity and depth images are jointly combined to contribute to the SR reconstruction of both depth map and intensity images.

In Fig. 1 we show an overview of our multi-frame SR technique for the ToF imaging. First, a set of LR pairs of intensity (real, positive) images and depth maps are acquired simultaneously by a ToF camera. A phasor representation combines the intensity and depth information measured at each pixel from the ToF camera into a complex valued LR image. Finally, the SR method proposed in [15], is applied to a set of complex valued LR images to generate SR intensity and depth images simultaneously.

The rest of the paper is organized as follows. In section 2 we introduce the ToF acquisition system. In section 3 we introduce the SR algorithm for ToF images. Experimental results on real datasets are presented in section 4. Finally, section 5 concludes the paper.

2. TIME-OF-FLIGHT IMAGING

2.1. ToF imaging principle

ToF is an active imaging technique which encodes both intensity and depth information of a scene into each captured image. We illustrate the ToF acquisition scheme in Fig. 2. Both the light source and the shutter of the ToF camera are amplitude-modulated, typically at the same frequency ω. The light source output is represented as $m(t)$ and the shutter coding as $r(t-\psi)$, where ψ is an arbitrary phase delay introduced at the shutter. The modulated light $m(t)$ travels through space and is reflected by an object, and then it reaches the camera sensor at pixel p. The light received will retain amplitude modulation frequency ω, but it will be phase delayed by $\phi_p = \frac{\omega d_p}{2c}$ and attenuated by $a_p m(t-\phi_p)$, where d_p is the distance of the object at position p, c is the speed of the light constant, and a_p is the albedo.

The sensor measurement at the pixel p and phase delay ψ, for an exposure duration of T, is given as:

$$B(p,\psi) = \int_{t=0}^{T} a_p m(t-\phi_p) r(t-\psi) dt \tag{1}$$

By varying the delay ψ, one can capture the entire correlation between the reflected signal and the exposure signal. Most ToF sensors use only four measurements (referred as quadrature measurements) that correspond to $\psi = 0, \pi/2, \pi, 3\pi/2$, to recover the amplitude a_p and the phase ϕ_p of the reflected signal as

$$a_p = \sqrt{\frac{[B(p,3\pi/2) - B(p,\pi/2)]^2 + [B(p,\pi) - B(p,0)]^2}{2}}, \tag{2}$$

$$\phi_p = \arctan\left(\frac{B(p,3\pi/2) - B(p,\pi/2)}{B(p,\pi) - B(p,0)}\right). \tag{3}$$

Where the intensity value for the pixel p is given by the amplitude value a_p, and the depth value at the same pixel can be easily calculated as $d_p = \frac{2c\phi_p}{\omega}$.

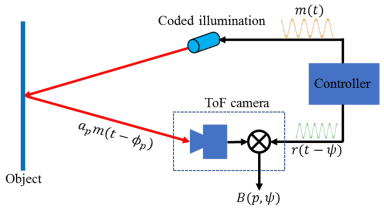

Fig. 2. **ToF depth imaging (assume single depth):** The computer sends out two signals: $m(t)$ to control the laser diode and $r(t-\psi)$ as reference to ToF sensor. The reflection from object ($a_p m(t-\phi_p)$) is collected by ToF pixels, and then correlates with the reference signal ($r(t-\psi)$) to generate the camera's output.

2.2. Linear forward model for ToF

Clearly, according to the ToF forward model above, the amplitude and phase are non-linearly related to the correlational measurements. For example, assume two ToF pixels p_1 and p_2 with corresponding amplitude and phase of (a_{p_1}, ϕ_{p_1}) and (a_{p_2}, ϕ_{p_2}). If we combine p_1 and p_2 to form a super-pixel p, the resulting amplitude and the phase at the super-pixel is not $(a_{p_1} + a_{p_2}, \phi_{p_1} + \phi_{p_2})$.

Using a phasor representation [18], the output of a ToF camera can be represented as a complex matrix $\mathbf{Y} \in \mathbb{C}^{M\times N}$. Similarly, we model the original scene as a complex matrix $\mathbf{X} \in \mathbb{C}^{kM\times kN}$ (k represents the magnification factor).

$$\mathbf{Y}(p) = a_p e^{i\phi_p}, \quad \mathbf{X}(P) = A_P e^{i\Phi_P}, \tag{4}$$

where $i = \sqrt{-1}$, p stands for pixel p on the ToF sensor. A_P and Φ_P represent the amplitude and phase on the scene at point P.

Now, we can use this phasor representation to build the linear measurement model from the scene to the ToF sensor.

3. MULTI-FRAME SR FOR TOF IMAGING

Let $\mathbf{Y}_1, \ldots, \mathbf{Y}_L \in \mathbb{C}^{MN\times 1}$ be the phasor representations of a sequence of L LR frames acquired by a ToF camera, written as column vectors. Let us assume the phasor representation of the HR frame that we want to recover is $\mathbf{X} \in \mathbb{C}^{k^2MN\times 1}$ written as a column vector, where k is the magnification factor. In this work we perform SR on the real and imaginary parts separately. To simplify the notation we define $\mathbf{y}_l \in \{\mathrm{Re}(\mathbf{Y}_l), \mathrm{Im}(\mathbf{Y}_l)\}$ and $\mathbf{x} \in \{\mathrm{Re}(\mathbf{X}), \mathrm{Im}(\mathbf{X})\}$, and assume the following degradation model

$$\mathbf{y}_l = \mathbf{D}\mathbf{W}_l\mathbf{x} + \mathbf{n}_l \quad l = 1, \ldots, L, \tag{5}$$

where $\mathbf{D} \in \mathbb{R}^{MN\times k^2MN}$ is a known downsampling matrix, $\mathbf{W}_l \in \mathbb{R}^{k^2MN\times k^2MN}$ is a warping matrix which models the movement between the HR image $\mathbf{x}$ and the HR version of l-th frame $\mathbf{y}_l$, and $\mathbf{n}_l \in \mathbb{R}^{MN\times 1}$ is additive noise term. We assume that the warping matrices $\mathbf{W}_l, l = 1, \ldots, L$, are not known, and they are estimated jointly with the HR image $\mathbf{x}$.

Assuming each $\mathbf{n}_l, l = 1, \ldots, L$, represents Gaussian noise with zero mean and the same covariance matrix given by $\beta^{-1}\mathbf{I}$, we obtain the following probability distribution on the observations

$$\mathrm{p}(\mathbf{y}_1, \ldots, \mathbf{y}_L | \mathbf{x}, \mathbf{W}_1, \ldots, \mathbf{W}_L, \beta) \propto \beta^{LMN/2} \exp\left\{-\frac{\beta}{2}\sum_{l=1}^{L} \|\mathbf{y}_l - \mathbf{D}\mathbf{W}_l\mathbf{x}\|^2\right\} \tag{6}$$

A Total Variation (TV) prior model [19] is assumed on the solution to enforce piecewise smoothness

$$\mathrm{p}(\mathbf{x}|\alpha) \propto \alpha^{NM/2} \exp\left\{-\alpha \sum_{j=1}^{NM} \sqrt{\Delta_j^h(\mathbf{x})^2 + \Delta_j^v(\mathbf{x})^2}\right\}, \quad (7)$$

where $\Delta_j^h(\mathbf{x})$ and $\Delta_j^v(\mathbf{x})$ represent the horizontal and vertical gradients of $\mathbf{x}$ at pixel j, respectively, and α is a precision parameter to be estimated. Finally, non-informative flat priors are used for $\mathrm{p}(\mathbf{W}_l), l = 1, \ldots, L$, $\mathrm{p}(\alpha)$ and $\mathrm{p}(\beta)$.

Our goal is to calculate the posterior distribution of the unknowns given the observations, which can be written using Bayes' rule as

$$\mathrm{p}(\mathbf{x}, \mathbf{W}_1, \ldots, \mathbf{W}_L, \alpha, \beta|\mathbf{y}_1, \ldots, \mathbf{y}_L) = \quad (8)$$
$$\frac{\mathrm{p}(\mathbf{y}_1, \ldots, \mathbf{y}_L|\mathbf{W}_1, \ldots, \mathbf{W}_L, \beta)\mathrm{p}(\mathbf{x}|\alpha)\prod_{l=1}^{L}\mathrm{p}(\mathbf{W}_l)\mathrm{p}(\alpha)\mathrm{p}(\beta)}{\mathrm{p}(\mathbf{y}_1, \ldots, \mathbf{y}_L)}.$$

In this case, however, we cannot explicitly calculate $\mathrm{p}(\mathbf{y}_1, \ldots, \mathbf{y}_L)$ and therefore we do not have access to the posterior distribution. To alleviate this problem we apply the method proposed in [15] where the posterior distribution is approximated by minimizing the Kullback-Leibler divergence (see [15] for details). The posterior distribution is approximated as a product of probability distributions

$$\mathrm{p}(\mathbf{x}, \mathbf{W}_1, \ldots, \mathbf{W}_L, \alpha, \beta|\mathbf{y}_1, \ldots, \mathbf{y}_L) \approx \mathrm{q}(\mathbf{x}) \prod_{l=1}^{L} \mathrm{q}(\mathbf{W}_l)\mathrm{q}(\alpha)\mathrm{q}(\beta). \quad (9)$$

By integrating with respect to $\mathbf{W}_l, l = 1, \ldots, L$, α and β, we find the posterior marginal of the HR image $\mathrm{q}(\mathbf{x})$, which is a Gaussian distribution. Finally, the HR image is estimated as the mean of $\mathrm{q}(\mathbf{x})$. Notice that, since $\mathrm{q}(\mathbf{x})$ is a Gaussian distribution, mode and mean coincide.

In our experiments we use a Matlab© implementation, provided by the authors of [15], which is available in the website http://decsai.ugr.es/pi/superresolution/software.html.

4. EXPERIMENTAL RESULTS

In this section, the proposed method is evaluated on both simulated and real examples. In addition, we compare the performance with the baseline method of bicubic interpolation. All experiments were carried out on a desktop Windows© PC with Intel© i7 CPU and 64GB RAM running MATLAB©.

4.1. Simulation

To demonstrate the multi-frame SR for the ToF imaging, we fist perform a simulation experiment. A 3D scene with ground truth depth is chosen from the well-known Middlebury Dataset [20]. The ground-truth dataset has 1154× 912 pixels, and we assume the low resolution measurement is 288 × 231 pixels with the magnification factor of 4. The warping matrix is achieved by shifting in horizontal and vertical axes and rotating the ground-truth scene. The horizontal and vertical shifts are randomly generated with values between -10 and 10 pixels. The rotation is also randomly generated each time with value between -7 and 7 degrees. The low resolution measurement is produced based on the imaging model including adding warping and down-sampling as described above, and nine LR ToF measurements are generated and used for the multi-frame SR reconstruction. A Gaussian noise with 30 dB SNR is added for the ToF measurements in the simulation.

We used the reconstruction algorithm to generate the high resolution image for the real and imaginary part, and then combine them to generate the intensity and depth images. Figs. 3(a-c) show the ground truth depth, the bicubic interpolation of the LR ToF depth, and multi-frame SR reconstruction depth. As we can observe in the close-up marked with red box, fine details of the "pen tip" in multi-frame SR reconstruction is better recovered than that in the bicubic interpolation. The same phenomena is observed in intensity images (Figs. 3(d-f)). More details of the letters can be observed from the multi-frame SR intensity image (Fig. 3(f)) compared to that from the bicubic interpolation (Fig. 3(e)).

Table 1 shows the PSNR obtained by the intensities images. The proposed method outperforms bicubic interpolation by more than 3 dB. To measure the error in depth images, table 1 shows the Root Mean Squared Error (RMSE). The proposed method obtains an improvement of almost 10 cm in depth over bicubic interpolation. Computational times are also reported in table 1. We can observe the proposed method has a high computational cost compared to bicubic interpolation. However we expect to reduce the processing time by optimizing the processing algorithms and utilizing GPU acceleration [21].

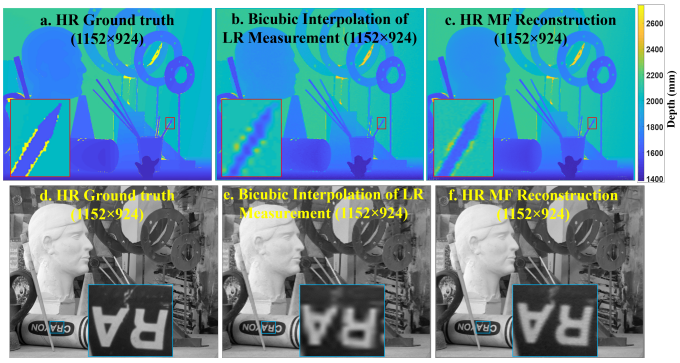

Fig. 3. **Simulation results of multi-frame SR for ToF imaging : (a)** The ground truth of the scene from the Middlebury Dataset. **(b)** The bicubic interpolation of one LR ToF depth measurement. **(c)** The multi-frame SR reconstruction with nine LR measurements. The colorbar shows the depth in mm. **(d-f)** show the ground truth, the bicubic interpolation of one LR ToF intensity measurement, and multi-frame SR reconstruction with nine measurements, respectively. Red boxes show the close-up depth images of the "pen tip". Blue boxes show the close-up intensity images of the letters.

	Bicubic	Proposed Method
Intensities (PSNR)	17.9 dB	21.1 dB
Depths (RMSE)	30.3 cm	20.6 cm
Time	$<$ 1 minute	15 minutes

Table 1. Figures of merits obtained by bicubic interpolation and proposed method in simulations.

4.2. Experiments

To evaluate the proposed framework, we perform a real-world experiment with an off-the-shelf ToF sensor with 320×240 pixels (OPT8241, Texas Instrument). The ToF sensor captures 3D objects with various distances of about 0.5 m to 1m from the sensor. During the experiment, the camera is handheld, and a video is recorded by moving the camera. 25 frames from the recorded video are used for

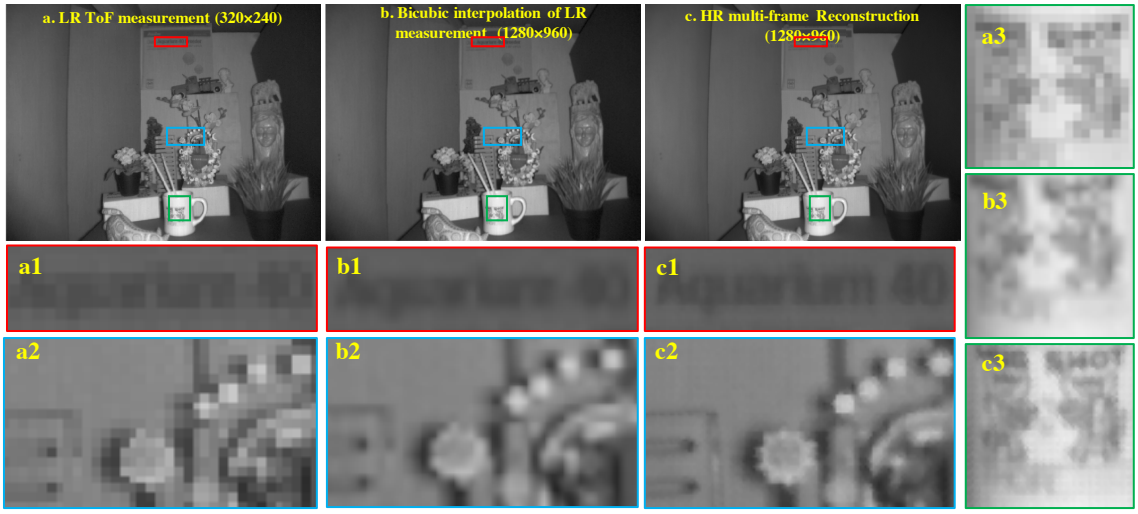

Fig. 4. **Multi-frame SR intensity image for ToF sensor: (a-c)** show the original LR ToF measurement (Enlarged for visualization), the bicubic interpolation of LR ToF measurement, and the multi-frame SR reconstruction, respectively. Twenty-five LR ToF measurements are used for the SR reconstruction. Color boxes show closeup images of objects at different locations correspondingly.

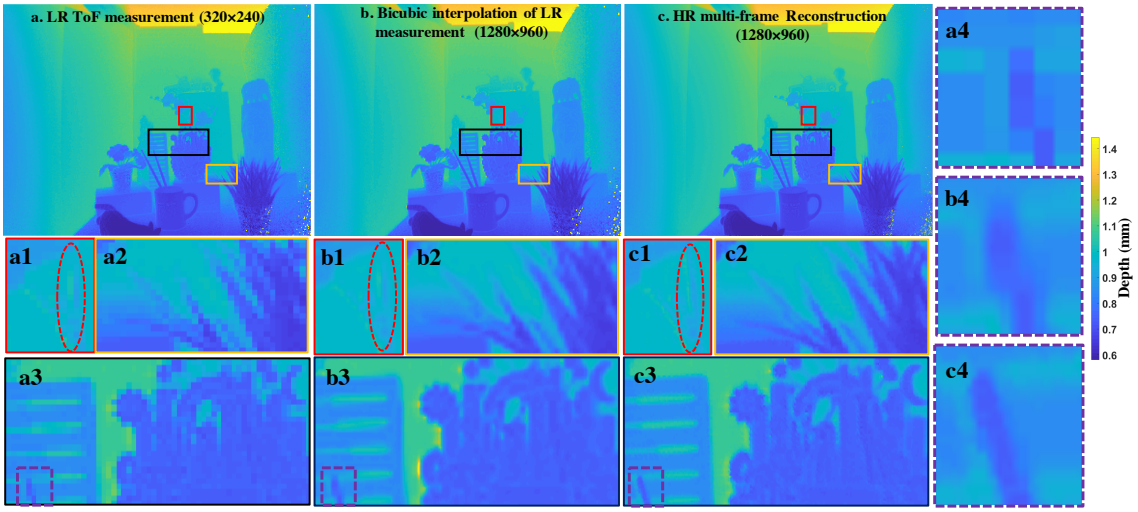

Fig. 5. **Multi-frame SR depth image for ToF sensor: (a-c)** show the original LR ToF measurement (Enlarge for visualization), the bicubic interpolation of LR ToF measurement, and the multi-frame SR reconstruction. Twenty-five LR ToF measurements are used for the SR reconstruction. Color boxes show closeup images of objects at different locations correspondingly. The colorbar shows the depth information.

the multi-frame SR reconstruction. We use the TV reconstruction algorithms for the reconstruction with results shown in Figs. 4 and 5.

Figs. 4(a-c) show the original LR ToF measurement, the bicubic interpolation, and the multi-frame SR reconstruction, respectively. The color boxes show three closeup images from objects at different locations to the sensor, and more details can be seen in Fig. 4(c). For instance, letters of "SHOT" on the mark cup can be clearly visualized in Fig. 4(c3), but hardly to differentiate in Fig. 4(b3) or (a3).

In the depth images, fine details in multi-frame SR reconstruction (Fig 5(c)) can be visualized compared to that in LR ToF measurement (Fig 5(a)) and in the bicubic interpolation (Fig. 5(b)). For example, branches of the flower (marked with red dash circle) in Fig. 5(c1) can be fully visualized but failed in Figs. 5(a1 and b1). Another example is tips of the little stick in close-up images (purple dash boxes) of Figs. 5(a3, b3, c3). We can see the sharp tip in Fig. 5(c4), but fail to see its shapes in Figs. 5(a4 and b4). The same phenomena can be observed in Fig. 5(c2) compared to that in Figs. 5(a2 and b2).

5. CONCLUSIONS

Current ToF sensors have low spatial resolution compared to regular CCD/CMOS sensors due to fabrication limitations. In this work, we have proposed a novel method to improve the spatial resolution of ToF images. To summarize, we have expressed the ToF imaging as a complex-output imaging model with phasor resulting in a linear forward measurement model. We then extended the multi-frame SR technique to our model and optimized the intensity and phase information jointly. Higher spatial resolution in intensity and depth images are both achieved in the reconstruction images. We believe this provides a simple solution to improve the spatial resolution of ToF sensors.

6. REFERENCES

[1] Richard Hartley and Andrew Zisserman, *Multiple View Geometry in Computer Vision*, Cambridge University Press, New York, USA, 2 edition, 2003.

[2] David J. Kriegman, Ernst Triendl, and Thomas O. Binford, "Stereo vision and navigation in buildings for mobile robots," *IEEE Transactions on Robotics and Automation*, vol. 5, no. 6, pp. 792–803, 1989.

[3] Zhengyou Zhang, "Microsoft kinect sensor and its effect," *IEEE MultiMedia*, vol. 19, no. 2, pp. 4–10, 2012.

[4] Fengqiang Li, Ting Xu, Duc-Huy T. Nguyen, Xiaolei Huang, Christopher S. Chen, and Chao Zhou, "Label-free evaluation of angiogenic sprouting in microengineered devices using ultrahigh-resolution optical coherence microscopy," *Journal of biomedical optics*, vol. 19, no. 1, pp. 016006–016006, 2014.

[5] Claus Weitkamp, *Lidar: range-resolved optical remote sensing of the atmosphere*, vol. 102, Springer Science & Business, 2006.

[6] Jason Geng, "Structured-light 3d surface imaging: a tutorial," *Advances in Optics and Photonics*, vol. 3, no. 2, pp. 128–160, 2011.

[7] Chia-Kai Yeh, Nathan Matsuda, Xiang Huang, Fengqiang Li, Marc Walton, and Oliver Cossairt, "A streamlined photometric stereo framework for cultural heritage," in *European Conference on Computer Vision*. Springer, 2016, pp. 738–752.

[8] Aggelos K. Katsaggelos, Rafael Molina, and Javier Mateos, *Super Resolution of Images and Video*, Morgan & Claypool, 2007.

[9] Changpeng Ti, Ruigang Yang, James Davis, and Zhigeng Pan, "Simultaneous time-of-flight sensing and photometric stereo with a single tof sensor," in *Proceedings of the IEEE Conference on Computer Vision and Pattern Recognition*, 2015, pp. 4334–4342.

[10] Achuta Kadambi, Vage Taamazyan, Boxin Shi, and Ramesh Raskar, "Polarized 3d: High-quality depth sensing with polarization cues," in *Proceedings of the IEEE International Conference on Computer Vision*, 2015, pp. 3370–3378.

[11] Tak-Wai Hui, Chen Change Loy, and Xiaoou Tang, "Depth map super-resolution by deep multi-scale guidance," in *European Conference on Computer Vision*. Springer, 2016, pp. 353–369.

[12] Fengqiang Li, Huaijin Chen, Adithya Pediredla, Chiakai Yeh, Kuan He, Ashok Veeraraghavan, and Oliver Cossairt, "Cs-tof: High-resolution compressive time-of-flight imaging," *Optics Express*, vol. 25, no. 25, pp. 31096–31110, 2017.

[13] Lei Xiao, Felix Heide, Matthew O'Toole, Andreas Kolb, Matthias B. Hullin, Kyros Kutulakos, and Wolfgang Heidrich, "Defocus deblurring and superresolution for time-of-flight depth cameras," in *Proceedings of the IEEE Conference on Computer Vision and Pattern Recognition*, 2015, pp. 2376–2384.

[14] Sina Farsiu, Dirk Robinson, Michael Elad, and Peyman Milanfar, "Fast and Robust Multi-Frame Super-Resolution," *IEEE Transactions on Image Processing*, vol. 13, no. 10, pp. 1327–1344, 2004.

[15] S. Derin Babacan, Rafael Molina, and Aggelos K. Katsaggelos, "Variational Bayesian Super Resolution.," *IEEE Transactions on Image Processing*, vol. 20, no. 4, pp. 984–999, 2011.

[16] "See better and further with super res zoom on the pixel 3," `https://ai.googleblog.com/2018/10/see-better-and-further-with-super-res.html`, Google AI Blog, 15 Oct. 2018.

[17] Jaesik Park, Hyeongwoo Kim, Yu-Wing Tai, Michael S Brown, and Inso Kweon, "High quality depth map upsampling for 3d-tof cameras," in *2011 International Conference on Computer Vision*, Nov 2011, pp. 1623–1630.

[18] Mohit Gupta, Shree K. Nayar, Matthias B. Hullin, and Jaime Martin, "Phasor imaging: A generalization of correlation-based time-of-flight imaging," *ACM Transactions on Graphics (ToG)*, vol. 34, no. 5, pp. 156, 2015.

[19] Leonid I. Rudin, Stanley Osher, and Emad Fatemi, "Nonlinear total variation based noise removal algorithms," *Physica D: Nonlinear Phenomena*, vol. 60, no. 1, pp. 259 – 268, 1992.

[20] Daniel Scharstein and Richard Szeliski, "High-accuracy stereo depth maps using structured light," in *Proceedings of the 2003 IEEE Computer Society Conference on Computer Vision and Pattern Recognition*, 2003.

[21] Yutaka Endo, Tomoyoshi Shimobaba, Takashi Kakue, and Tomoyoshi Ito, "Gpu-accelerated compressive holography," *Optics Express*, vol. 24, no. 8, pp. 8437–8445, 2016.